JPE 15-6-5

http://dx.doi.org/10.6113/JPE.2015.15.6.1456
ISSN(Print): 1598-2092 / ISSN(Online): 2093-4718

A Control Strategy Based on Small Signal Model for Three-Phase to Single-Phase Matrix Converters

Si Chen[†], Hongjuan Ge[*], Wenbin Zhang[*], and Song Lu[*]

[†,*]College of Automation Engineering, Nanjing University of Aeronautics and Astronautics, Nanjing, China

Abstract

This paper presents a novel close-loop control scheme based on small signal modeling and weighted composite voltage feedback for a three-phase input and single-phase output Matrix Converter (3-1MC). A small non-polar capacitor is employed as the decoupling unit. The composite voltage weighted by the load voltage and the decoupling unit voltage is used as the feedback value for the voltage controller. Together with the current loop, the dual-loop control is implemented in the 3-1MC. In this paper, the weighted composite voltage expression is derived based on the sinusoidal pulse-width modulation (SPWM) strategy. The switch functions of the 3-1MC are deduced, and the average signal model and small signal model are built. Furthermore, the stability and dynamic performance of the 3-1MC are studied, and simulation and experiment studies are executed. The results show that the control method is effective and feasible. They also show that the design is reasonable and that the operating performance of the 3-1MC is good.

Key words: Closed-loop control, Power decoupling, Small signal model, Three-phase to Single-phase Matrix Converter

I. INTRODUCTION

The alternative part of the output power in a three-phase to single-phase Matrix Converter (3-1MC) causes input current distortions and power factor reductions, due to the direct coupling between the input and output [1]-[3]. Paper [4] proposed a modulation method where the power pulsation in the output side was absorbed by the inertia of the rotor. However, this method increased the mechanical loss of the motor and reduced the efficiency of the power generation system. In [5], most of the power pulsation was stored in the Z-source impedance network. However, some part of the power pulsation still impacted the input side.

A method where the active power decoupling unit is used to compensate the power pulsation has been shown to be more effective and feasible [6]-[9]. Makoto Saito proposed the concept of active power decoupling in 2004, where single-phase power pulsations were stored in an inductor by modulation of the power switches. To reduce the bulk of the decoupling unit, the large inductor was replaced by a capacitor, and a novel single-phase to three-phase MC topology was developed in [7]. Furthermore, [8] investigated the design principle of the decoupling capacitor. Then, a simple decoupling method in which a non-polar capacitor was used as a decoupling unit was introduced in [9], and the corresponding modulation strategy was discussed.

A 3-1MC, which is in parallel to the grid, was studied and designed as a constant-current source in [10]. The input current and output current of the converter were controlled independently. The reference value of the input current controller was calculated by the output power in the grid side, and the power loss is not taken into account. Meanwhile, the regulating algorithm was implemented according to the effective value. Consequently, its accuracy and dynamic performance were not good. This paper presents a novel control method where the composite voltage, which is weighted by its load voltage and decoupling unit voltage, is used as the feedback value. With its instantaneous output voltage control, the novel method makes the performance of the 3-1MC better.

Control system design based on the small signal model has not been studied a lot for 3-1MCs. Unlike 3-3MCs, in which the output voltage can be decomposed into d and q components and the small signal model can be established simply based on them, the modeling of 3-1MCs is much more

Manuscript received Feb. 5, 2015; accepted May 21, 2015
Recommended for publication by Associate Editor Sangshin Kwak.
[†]CorrespondingAuthor:chensinuaa@163.com
Tel: +86-025-84896005, Nanjing Univ. of Aeronautics and Astronautics
[*]College of Automation Engineering, Nanjing University of Aeronautics and Astronautics, China

difficult. Based on the ideas of [11] and [12], a solution is presented here where the small signal model of a 3-1MC is built based on the composite voltage. With this idea, the dual-loop controllers are designed, and the prototype is developed. A series of simulation and experimental studies are executed to verify its effectiveness and feasibility.

II. POWER DECOUPLING UNIT

A. Power Decoupling Principles

The topology and the equivalent circuit of a 3-1MC are illustrated in Fig. 1and Fig. 2. The virtual ac-dc side is a three-phase voltage source type rectifier (VSR). Assuming that the input instantaneous power is constant and that the input current and voltage are in-phase, the dc link presents the properties of a constant current source [13]. The input power of the converter is equal to the dc link power in ideal conditions. Therefore, the dc link voltage must be maintained as a constant.

The virtual dc-ac side is a two-phase current source type inverter (CSI).SPWM is adopted in the load phase and in the active power decoupling phase. The modulation functions are assumed as:

$$\begin{cases} f_l = h_l^* \cos\omega_o t \\ f_c = h_c^* \sin(\omega_o t + \varphi_c) \end{cases} \tag{1}$$

According to the superposition theorem, the dc link voltage is the weighted sum of the load voltage and the decoupling capacitor voltage, i.e. the composite voltage u_{comp} satisfies:

$$\begin{aligned} u_{comp} &= f_l u_o + f_c u_c = \frac{h_l^* U_o}{\sqrt{2}} \cos\varphi_o + \\ &\frac{h_l^* U_o}{\sqrt{2}} \cos(2\omega_o t + \varphi_o) - \frac{h_c^{*2} i_{dc}}{2\omega_o C_c} \sin(2\omega_o t + 2\varphi_c) \end{aligned} \tag{2}$$

In (1) and (2), h_l^* and h_c^* are the modulation radios of the load phase and the decoupling phase, respectively, u_o is the load voltage, u_c is the decoupling capacitor voltage, ω_o is the output angular velocity, φ_c is the initial phase angle of the decoupling modulation wave, φ_o is the load impedance angle, U_o is the effective value of the load voltage, i_{dc} is the dc link current, and C_c is the capacitance of the decoupling capacitor. When h_c^* and φ_c satisfy formula (1-3)[14], pulsed voltage components of twice the output frequency are neutralized. Then, u_{comp} is maintained as a constant: $h_l^* U_{om} \cos\varphi_o / 2$.

$$\varphi_c = \frac{1}{4}\pi + \frac{\varphi_o}{2} \ , \ h_c^* = h_l^* \sqrt{\omega_o C_c |Z_o|} \tag{3}$$

Therefore, the single-phase power pulsation is decoupled with a constant input power, and the instantaneous input power is kept at a constant value, which can be expressed as:

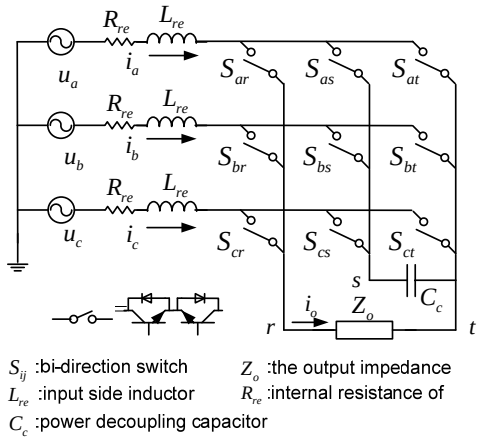

Fig. 1. 3-1MC with a power decoupling unit.

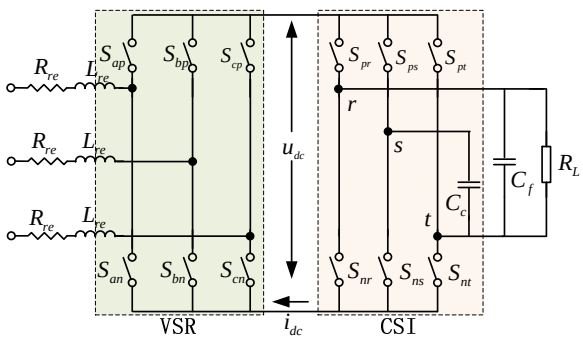

Fig. 2. Equivalent circuit of 3-1MC.

$$P_{in} = u_{comp} \times I_{dc} = \frac{1}{\sqrt{2}} h_l^* U_o I_{dc} \cos\varphi_o \tag{4}$$

B.Design of the Power Decoupling Unit

The power pulsation is absorbed and released completely by the decoupling capacitor in a pulsed period. Energy stored in the capacitor is equal to the work of the power pulsation. Then, the relationship between the capacitance of C_c and its maximum voltage $U_{c\max}$ can be expressed as[14]:

$$C_c = \frac{P_o}{\pi f_o U_{c\max}^2} \tag{5}$$

Where P_o is the load power, and f_o is the output frequency.

On the other hand, the converter usually works in the linear modulation range. Therefore, the sum of the load phase duty ratio d_l and the decoupling phase duty ratio d_c should be less than 1 in real time. Combining (1) with (3), the duty ratios:

$$\begin{cases} d_l = \left| h_l^* \cos\omega_o t \right| \\ d_c = h_l^* \sqrt{\omega_o C_c |Z_o|} \left| \sin(\omega_o t + \varphi_c) \right| \end{cases} \tag{6}$$

By using the Cosine theorem, the amplitude of the sum of the duty ratios satisfies:

$$\left| d_\Sigma \right| = \left| d_l + d_c \right| = h_l^* \sqrt{1 + \omega_o C_c |Z_o| + 2\sqrt{\omega_o C_c |Z_o|} \cos\varphi_c} \le 1 \tag{7}$$

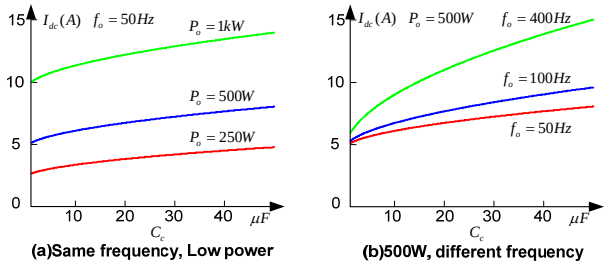

Fig. 3. Relation curves of capacitance and current stress.

TABLE I

CAPACITANCE OF C_c IN 5KW MATRIX CONVERTER

frequency /Hz	50	60	100	400
capacitance/μF	220	183	110	27.5

To improve the utilization rate of the power switches and the voltage transfer ratio, $|d_\Sigma|$ should be designed to be as large as possible. $|d_\Sigma|=1$ can be assumed here. Substitute (4) into (7). Then, the relationship between the dc link current and the capacitance of C_c is obtained as:

$$I_{dc}\approx\frac{\sqrt{2}P_o}{U_o\cos\varphi_o}\sqrt{1+\omega_o C_c\frac{U_o^2}{P_o}+2\sqrt{\omega_o C_c\frac{U_o^2}{P_o}}\cos\varphi_c} \quad (8)$$

Taking $U_o=150V$ as an example, the relationships between C_c and I_{dc} are presented in Fig. 3 for situations of different output powers and different output frequencies .The dc link current is increased when a larger capacitance is chosen and its value also grows with an increase of the power and frequency.

Combined with the limitation of (5), in low power appliance like 500W,50Hz, if the capacitance of C_c is chosen between $20\mu F$-$30\mu F$, the voltage stress and current stress are well balanced.

In relative high power application, the power pulsation can also be compensated by the decoupling capacitor in the same method, when the parameters of the modulation functions meet equation (3). Table I lists the design values of C_c at different output frequencies of the 5kW matrix converter. The maximum voltage of the decoupling capacitor is designed as about 400V.

III. MODULATION OF THE 3-1 MC

After increasing the power decoupling unit, a modulation method that synthesizes the modulation of the VSR and the CSI is adopted for the 3-1 MC.

A. SVPWM Modulation for VSR

For the VSR, SVPWM is applied [15], [16]. Fig. 4 shows the voltage space of the VSR input side. It is divided into six sectors by six basic vectors, and the amplitude of each

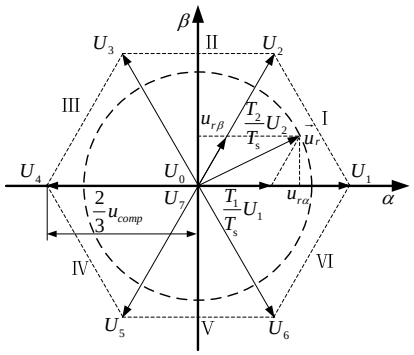

Fig. 4.Voltage vector diagram of MC input side.

basic vector is $2u_{comp}/3$ .In order to implement the unit power factor, the three-phase input voltages need to be symmetrical sinusoidal voltages.

Namely the space vector $\vec{u}_r$ rotates at a constant speed in the $\alpha\beta$ static coordinate system. Therefore, the rotation vector $\vec{u}_r$ in each sector can be composited by the adjacent basic vectors, and the trajectory of its endpoint is an approximate voltage cycle.

According to the voltage vector synthesis relationship and the sine theorem [17], the operating times T_{i1} *and* T_{i2} of the basic vectors U_{i1} *and* U_{i2} in each sector can be obtained in Table II. T_{i0} is the operating time of the zero vector which can be calculated as: $T_{i0}=T_s-T_{i1}-T_{i2}$.

By detecting the sector signal of the vector $\vec{u}_r$, the operating voltage vectors in each sector and their operating times are determined. Then, the VSR is modulated to make the virtual dc link perform as a current source.

B. Staggered Modulation for CSI

For the CSI, when the load phase and decoupling phase work together, simultaneous conduction of the same pole side switches (S_{ps} , S_{pr}) and (S_{ns} , S_{nr}) must be avoided. Otherwise two capacitors with different voltages connect in parallel, and the short circuit current will breakdown the power switches (as shown in Fig. 5). Thus, staggered modulation is carried out for the CSI.

SPWM is adopted for both phases and their modulation functions are given by (1). In order to implement staggered modulation, the duty ratios of the load phase and decoupling phase should be reasonably allocated to assure that the conducting time of the bridge arms(S_{pr},S_{nr})and(S_{ps},S_{ns}) do not overlap.

Where U_{i1} *lag* U_{i2} , T_s is PWM period , $u_{r\alpha}$, $u_{r\beta}$ are the value of $\vec{u}_r$ in $\alpha\beta$ static coordinate system.

Therefore, the carrier contains a couple of opposite triangular waves. The bridge arm (S_{pr},S_{nr}) is modulated by

TABLE II
OPERATING TIME OF VECTORS IN EACH SECTOR

Sector	I	II	III
Operating time of U_{i1} and U_{i2}	$T_{i1}=\frac{3T_s}{2(f_l u_o+f_c u_c)}(u_{r\alpha}-\frac{u_{r\beta}}{\sqrt{3}})$ $T_{i2}=\frac{\sqrt{3}u_{r\beta}T_s}{f_l u_o+f_c u_c}$	$T_{i1}=\frac{3T_s}{2(f_l u_o+f_c u_c)}(u_{r\alpha}+\frac{u_{r\beta}}{\sqrt{3}})$ $T_{i2}=\frac{3T_s}{2(f_l u_o+f_c u_c)}(\frac{u_{r\beta}}{\sqrt{3}}-u_{r\alpha})$	$T_{i1}=\frac{\sqrt{3}u_{r\beta}T_s}{f_l u_o+f_c u_c}$ $T_{i2}=-\frac{3T_s}{2(f_l u_o+f_c u_c)}(u_{r\alpha}+\frac{u_{r\beta}}{\sqrt{3}})$
Sector	V	VI	IV
Operating time of U_{i1} and U_{i2}	$T_{i1}=\frac{3T_s}{2(f_l u_o+f_c u_c)}(\frac{u_{r\beta}}{\sqrt{3}}-u_{r\alpha})$ $T_{i2}=-\frac{\sqrt{3}u_{r\beta}T_s}{f_l u_o+f_c u_c}$	$T_{i1}=-\frac{3T_s}{2(f_l u_o+f_c u_c)}(u_{r\alpha}+\frac{u_{r\beta}}{\sqrt{3}})$ $T_{i2}=-\frac{3T_s}{2(f_l u_o+f_c u_c)}(\frac{u_{r\beta}}{\sqrt{3}}-u_{r\alpha})$	$T_{i1}=-\frac{\sqrt{3}u_{r\beta}T_s}{f_l u_o+f_c u_c}$ $T_{i2}=\frac{3T_s}{2(f_l u_o+f_c u_c)}(u_{r\alpha}+\frac{u_{r\beta}}{\sqrt{3}})$

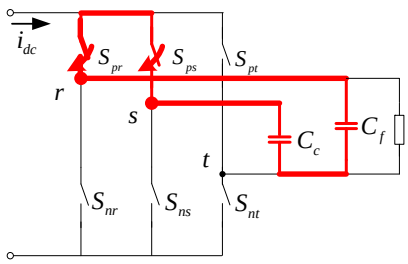

Fig. 5. Short circuit fault.

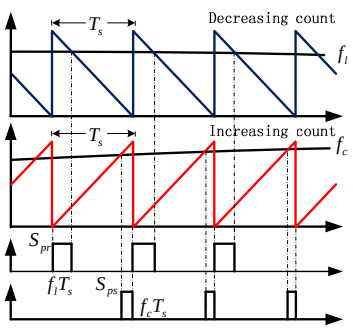

Fig. 6. Staggered modulation for CSI.

the decreasing-count triangle wave, while the bridge arm (S_{ps}, S_{ns}) is modulated by the increasing-count triangle wave. Then, the operating time of the two phases is allotted from two ends of a PWM period, as shown in Fig. 6.

In addition, the sum of the duty ratios of the two phases should be less than 1.The amplitude of the sum of the duty ratios $|d_\Sigma|$ meets equation (7):

$$|d_\Sigma| = h_l^* \sqrt{1+\omega_o C_c |Z_o| + 2\sqrt{\omega_o C_c |Z_o|}\cos\varphi_c} \le 1$$

The modulation ratio h_l^* is a constant. Therefore, $|d_\Sigma|$ has a positive correlation relationship with C_c when the load Z_o remains unchanged. Only when C_c is less than the limit value given by (8), can the requirement of $|d_\Sigma| \le 1$ can be guaranteed. In this case, the zero current state is always existent. Table III shows the time distribution in a PWM

TABLE III
TIME DISTRIBUTION FOR CSI

	Operating time
Load phase	0 *to* $\left|h_l^* \cos\omega_o t\right| T_s$
Zero Current State	$\left|h_l^* \cos\omega_o t\right| T_s$ *to* $\left(1-h_l^*\sqrt{\omega_o C_c \lvert Z_o\rvert}\left|\sin(\omega_o t+\varphi_c)\right|\right)T_s$
Decoupling phase	$\left(1-h_l^*\sqrt{\omega_o C_c \lvert Z_o\rvert}\left|\sin(\omega_o t+\varphi_c)\right|\right)T_s$ *to* T_s

period for the CSI.

As for the current type inverter, when only the load phase operates, the CSI's input voltage component is $f_l u_o$:

$$f_l u_o = f_l^2 \cdot i_{dc} \cdot Z_o = \frac{h_l^* U_o}{\sqrt{2}}\cos\varphi_o + \frac{h_l^* U_o}{\sqrt{2}}\cos(2\omega_o t+\varphi_o) \quad (9)$$

There is a low frequency pulsed component. If this pulsed component directly reflects the input side, it will cause input current distortion.

When only the decoupling phase operates, the CSI's input voltage component $f_c u_c$ happens to be a pulsed component of twice the output frequency.

$$f_c u_c = f_c \cdot \frac{1}{C_c}\int f_c i_{dc} dt = -\frac{h_c^{*2} i_{dc}}{2\omega_o C_c}\sin(2\omega_o t+2\varphi_c) \quad (10)$$

However, actual operation of the CSI should combine the load phase and the decoupling phase, so that the input voltage of the CSI is a composite voltage u_{comp} .When the modulation function satisfies (3), u_{comp} is simplified as:

$$u_{comp} = f_l u_o + f_c u_c = \frac{h_l^* U_o}{\sqrt{2}}\cos\varphi_o = \frac{1}{2}h_l^{*2} i_{dc}|Z_o|\cos\varphi_o \quad (11)$$

In (11), the low frequency pulsed component is eliminated and the composite voltage maintains constant.

Using the described modulation method, the current and voltage vector diagram of the CSI output side is obtained as shown in Fig. 7. The current space is divided into 4 sectors according to the direction of the current. The γ axis and ψ

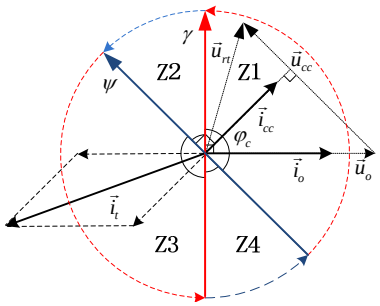

Fig. 7. Output current and voltage vectors of CSI.

axis are perpendicular to the load phase current vector and the decoupling phase current vector, respectively. The ψ axis lags the γ axis by φ_c. Combined with the VSR voltage space vector diagram, a 3-1MC with active power decoupling capacitor has a total of 6×4=24 kinds of sector combinations.

C. Switch Modes of the MC

After modulation synthesis, the operating time of each sector is reduced. When the operating vector of the VSR is U_{i1}, the conduction time of the load phase and decoupling phase are expressed as:

$$T_{o1} = d_l T_{i1} \quad T_{o2} = d_c T_{i1}$$

When the operating vector of the VSR turns into U_{i2}, the conduction time of the two phases change as:

$$T_{o3} = d_l T_{i2} \qquad T_{o4} = d_c T_{i2}$$

Therefore, the operating time of the zero vector can be calculated:

$$T_0 = T_s - T_{o1} - T_{o2} - T_{o3} - T_{o4}$$

Combining Table II and formula (6), 5 slices of the time signal of the 3-1 MC in all of the sectors are obtained.

To investigate working states of the 3-1 MC in different sectors, it is assumed that the input frequency is 50Hz and that the output frequency is 400Hz. Then, each voltage sector contains all of the current sectors. Table IV shows the power switch state of the 3-1 MC.

The 3-1MC has 5 kinds of switch modes in every sector combination. Take the VI—Z4 sector as an example to analyze the switch modes under the 5 time-slice signals (as illustrated in Fig. 8). Suppose time variables:

$$T_1 = T_{o1}\ ,\ T_2 = T_{o1} + T_{o2}\ ,\ T_3 = T_{o1} + T_{o2} + T_{o3}\ ,$$
$$T_4 = T_{o1} + T_{o2} + T_{o3} + T_{o4}$$

In mode (a), the inductor current of phase A and phase C discharge the load phase, while the decoupling capacitor energy remains unchanged. In mode (b), the inductors discharge the decoupling phase, whose charge current is the sum of the inductor currents of phase A and phase C, and filter capacitor discharges the load. In mode (c), the inductor current turns to discharge the load phase, but the charge current is the inductor current of phase A. In mode (d), the inductor current of phase A discharges the decoupling phase and the filter capacitor discharges the load. Mode (e) is the working state of the zero vector, in which the three phase inductors store energy.

TABLE IV
SWITCH STATES IN DIFFERENT KIND OF SECTOR COMBINATIONS

Sector	Vector	S_{ar}	S_{br}	S_{cr}	S_{as}	S_{bs}	S_{cs}	S_{at}	S_{bt}	S_{ct}
I—Z1	$U_{i1}-I_o$	1	0	0	0	0	0	0	1	1
	$U_{i1}-I_{cc}$	0	0	0	1	0	0	0	1	1
	$U_{i2}-I_o$	1	1	0	0	0	0	0	0	1
	$U_{i2}-I_{cc}$	0	0	0	1	1	0	0	0	1
	Zero	0	0	0	0	0	0	1	1	1
I—Z2	…	…								
…	…	…								
VI—Z4	$U_{i1}-I_o$	0	1	0	1	0	0	0	1	0
	$U_{i1}-I_{cc}$	0	0	0	0	1	0	1	0	1
	$U_{i2}-I_o$	0	1	1	0	0	0	1	0	0
	$U_{i2}-I_{cc}$	0	0	0	0	1	1	0	0	0
	Zero	1	1	1	0	0	0	0	0	0

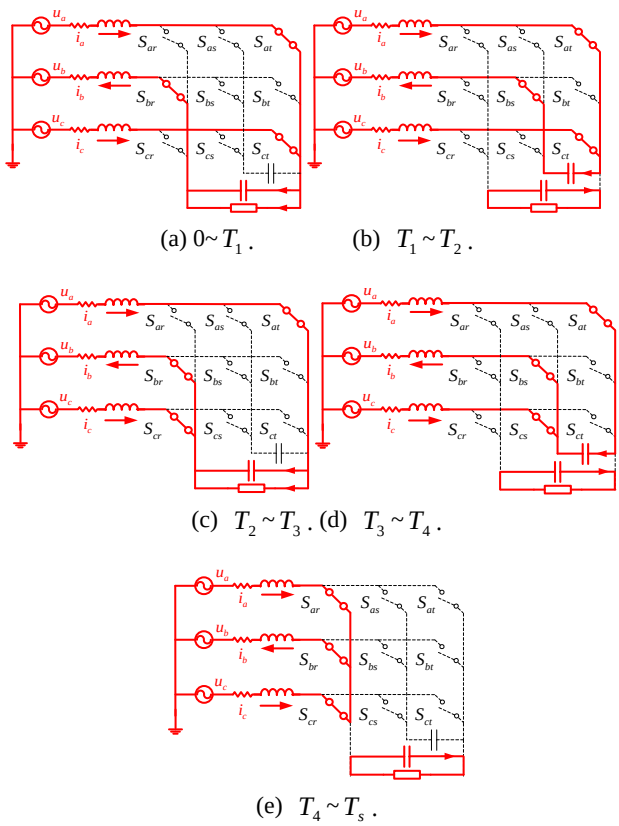

Fig. 8. Switching modes of 3-1MC in a PWM period.

As can be seen from the 5 kinds of switch modes, the current of the two phases with the largest amplitude charge the load and the power decoupling capacitor. This conforms to the law of voltage space vector modulation. The working state of the inductors and capacitors in the other sector combinations can be analyzed in the same way.

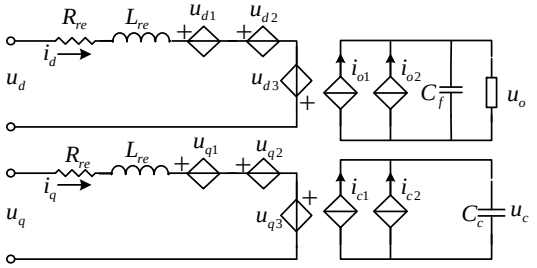

Fig. 9. Average signal model of 3-1MC.

IV. MODELING OF THE 3-1MC

A set of power switches and a decoupling capacitor are introduced into a 3-1MC, which increases the time-varying and nonlinear factors in the 3-1 MC mathematical model. In order to investigate the closed-loop control strategy, the average signal model of the 3-1MC is built in the dq coordinate system. Then, disturbances are separated to obtain a small signal model with the feed-forward decoupling control.

A. Average Signal Model

Combined with the equivalent circuit of the 3-1 MC power decoupling topology, the mathematical model of the VSR is derived by using the switch average model:

$$L_{re}\frac{d}{dt}\begin{bmatrix} i_a \\ i_b \\ i_c \end{bmatrix} = \begin{bmatrix} u_a \\ u_b \\ u_c \end{bmatrix} - R_{re}\begin{bmatrix} i_a \\ i_b \\ i_c \end{bmatrix} - \begin{bmatrix} u_{comp}(S_a - S^*) \\ u_{comp}(S_b - S^*) \\ u_{comp}(S_c - S^*) \end{bmatrix} \tag{12}$$

Where $S^* = (S_a + S_b + S_c)/3$ and $S_i (i = a,b,c)$ are switching functions.

KCL is applied for the CSI, and then the mathematical model can be expressed as:

$$\begin{cases} \dfrac{du_o}{dt} = \dfrac{1}{C_f}(f_l i_{dc} - \dfrac{u_o}{R_L}) = \dfrac{f_l(S_a i_a + S_b i_b + S_c i_c) - u_o/R_L}{C_f} \\ \dfrac{du_c}{dt} = \dfrac{1}{C_c} i_{cc} = \dfrac{f_c(S_a i_a + S_b i_b + S_c i_c)}{C_c} \end{cases} \tag{13}$$

Using formula (2), the state equation of the 3-1 MC power decoupling topology in static coordinates is deduced:

$$\dot{X} = AX + BU \tag{14}$$

$$X = \begin{bmatrix} i_a & i_b & i_c & u_o & u_c \end{bmatrix}^T, U = \begin{bmatrix} u_a & u_b & u_c & 0 & 0 \end{bmatrix}^T$$

$$B = diag\begin{bmatrix} 1/L_{re} & 1/L_{re} & 1/L_{re} & 0 & 0 \end{bmatrix}^T$$

$$A = \begin{bmatrix} -\dfrac{R_{re}}{L_{re}} & 0 & 0 & \dfrac{f_l(S^* - S_a)}{L_{re}} & \dfrac{f_c(S^* - S_a)}{L_{re}} \\ 0 & -\dfrac{R_{re}}{L_{re}} & 0 & \dfrac{f_l(S^* - S_b)}{L_{re}} & \dfrac{f_c(S^* - S_b)}{L_{re}} \\ 0 & 0 & -\dfrac{R_{re}}{L_{re}} & \dfrac{f_l(S^* - S_c)}{L_{re}} & \dfrac{f_c(S^* - S_c)}{L_{re}} \\ \dfrac{f_l S_a}{C_f} & \dfrac{f_l S_b}{C_f} & \dfrac{f_l S_c}{C_f} & -1/(C_f R_L) & 0 \\ \dfrac{f_c S_a}{C_c} & \dfrac{f_c S_b}{C_c} & \dfrac{f_c S_c}{C_c} & 0 & 0 \end{bmatrix}$$

In the static coordinates system, the average signal model of the 3-1MC is very intuitive and each variable has a clear physical meaning. However, the input current and voltage are ac variables, which is not conducive to control system designing and causes steady-state errors [18]. Therefore, the equivalent transformation matrix of the rotating coordinate system is employed:

$$T_{abc/dq} = \frac{2}{3}\begin{bmatrix} \cos\omega t & \cos(\omega t - \frac{2}{3}\pi) & \cos(\omega t + \frac{2}{3}\pi) \\ \sin\omega t & \sin(\omega t - \frac{2}{3}\pi) & \sin(\omega t + \frac{2}{3}\pi) \\ \frac{1}{2} & \frac{1}{2} & \frac{1}{2} \end{bmatrix}$$

Assuming that the three-phase input power is symmetrical, i.e. $i_a + i_b + i_c = 0$, $u_a + u_b + u_c = 0$, the state equation of the 3-1 MC power decoupling topology in the rotating coordinate system is derived as:

$$\dot{X}_{dq} = A_{dq}X_{dq} + B_{dq}U_{dq} \tag{15}$$

$$X_{dq} = \begin{bmatrix} i_d & i_q & u_o & u_c \end{bmatrix}^T , \ U_{dq} = \begin{bmatrix} u_d & u_q & 0 & 0 \end{bmatrix}^T$$

$$B_{dq} = diag\begin{bmatrix} 1/L_{re} & 1/L_{re} & 0 & 0 \end{bmatrix}^T$$

$$A = \begin{bmatrix} -\dfrac{R_{re}}{L_{re}} & \omega_i & -\dfrac{3f_l d_d}{2L_{re}} & -\dfrac{3f_c d_d}{2L_{re}} \\ -\omega_i & -\dfrac{R_{re}}{L_{re}} & -\dfrac{3f_l d_q}{2L_{re}} & -\dfrac{3f_c d_q}{2L_{re}} \\ \dfrac{3f_l d_d}{2C_f} & \dfrac{3f_l d_q}{2C_f} & -\dfrac{1}{C_f R_L} & 0 \\ \dfrac{3f_c d_d}{2C_c} & \dfrac{3f_c d_q}{2C_c} & 0 & 0 \end{bmatrix}$$

Where ω_i is the input angular velocity, d_d, d_q, i_d, i_q and u_d, u_q are the switching functions, input current and voltage in rotating coordinate system.

According to state equation (15), the average signal model of the 3-1MC in the dq coordinate system is illustrated in Fig. 9. To eliminate the time-varying factors caused by switches, the nonlinear switching elements are replaced by controlled sources which use the average components as control variables.

The voltage controlled sources of the input side:

$$u_{d1} = \frac{3}{2} f_l D_d u_o \ , \ u_{d2} = \frac{3}{2} f_c D_d u_c \ , \ u_{d3} = \omega_i L_{re} i_q$$

$$u_{q1} = \frac{3}{2} f_l D_q u_o \ , \ u_{q2} = \frac{3}{2} f_c D_q u_c \ , \ u_{q3} = \omega_i L_{re} i_d$$

The current controlled sources of the output side:

$$i_{o1} = \frac{3}{2} f_l D_d i_d \ , i_{o2} = \frac{3}{2} f_l D_q i_q \ , i_{c1} = \frac{3}{2} f_c D_d i_d \ i_{c2} = \frac{3}{2} f_c D_q i_q$$

Although the ac variables of the 3-1MC input side are turned into average dc components in the dq coordinate system, u_o and u_c in the output side are still ac variables. Therefore, it is necessary to use the composite voltage u_{comp} to express u_o and u_c, and to separate the disturbances to

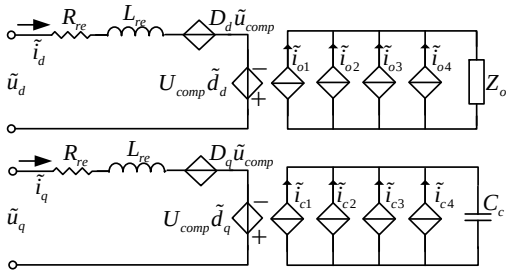

Fig. 10. Small signal circuit model of 3-1MC with feed-forward decoupling control.

obtain a linearized small signal model.

B. Small Signal Model

In order to eliminate time-varying variables, the disturbances of the references and high order small signal components are ignored, while only the disturbances from the input source and load are considered. The average signal variables in the average signal model are assumed as:

$x = X + \tilde{x}$, $x = \{i_d, i_q, d_d, d_q, u_d, u_q, u_{comp}, i_{dc}, u_o, u_c\}$. Insert x into (2). Then:

$$U_{comp} + \tilde{u}_{comp} = f_l\tilde{u}_o + f_c\tilde{u}_c + \frac{h_l^* U_o}{\sqrt{2}}\cos\varphi_o \tag{16}$$

The small signal components of the load voltage and decoupling capacitor voltage are:

$$\tilde{u}_o = h_l^*\tilde{i}_{dc}|Z_o|\cos(\omega_o t + \varphi_o) \tag{17}$$

$$\tilde{u}_c = -\frac{h_c^*\tilde{i}_{dc}}{\omega_o C_c}\cos(\omega_o t + \frac{1}{4}\pi + \frac{\varphi_o}{2}) \tag{18}$$

Combined with (16)-(18), the small signal component of the weighted composite voltage $\tilde{u}_{comp}$ is obtained as:

$$\tilde{u}_{comp} = f_l\tilde{u}_o + f_c\tilde{u}_c = \frac{h_l^{*2}}{2}\tilde{i}_{dc}|Z_o| \tag{19}$$

Formula (19) shows the linear relationship between $\tilde{u}_{comp}$ and $\tilde{i}_{dc}$ .The weighted composite voltage indirectly reflects the load voltage and decoupling capacitor voltage. As a result, $\tilde{u}_{comp}$ can be substituted for the ac variables u_o and u_c in the state equation of the 3-1 MC. Then, all of the ac components in the model are eliminated.

In the average signal model, the input d axis current and the q axis current are coupling. Thus, feed-forward decoupling control is employed to make the control circuits of the d axis and q axis mutually independent. According to the relationship between the input power references and the current references as Equation (20), the input unity power factor can be achieved if the reactive current reference is set to 0.

$$\begin{bmatrix} P_{in}^* \\ Q_{in}^* \end{bmatrix} = \frac{3}{2}\begin{bmatrix} U_m & 0 \\ 0 & U_m \end{bmatrix}\begin{bmatrix} I_d^* \\ I_q^* \end{bmatrix} = \frac{3}{2}\begin{bmatrix} U_m I_d^* \\ U_m I_q^* \end{bmatrix} \tag{20}$$

After the feed-forward decoupling control, all of the small signal components in (15) are separated. The differential equations of the d and q axis are deduced as follows:

$$\frac{d}{dt}\begin{bmatrix} \tilde{i}_d \\ \tilde{i}_q \end{bmatrix} = \begin{bmatrix} \frac{\tilde{u}_d}{L_{re}} \\ \frac{\tilde{u}_q}{L_{re}} \end{bmatrix} + \begin{bmatrix} \frac{-R_{re}}{L_{re}} & 0 & \frac{-3D_d}{2L_{re}} \\ 0 & \frac{-R_{re}}{L_{re}} & \frac{-3D_q}{2L_{re}} \end{bmatrix}\begin{bmatrix} \tilde{i}_d \\ \tilde{i}_q \\ \tilde{u}_{comp} \end{bmatrix} + \begin{bmatrix} \frac{-U_{comp}}{L_{re}} & 0 \\ 0 & \frac{-U_{comp}}{L_{re}} \end{bmatrix}\begin{bmatrix} \tilde{d}_d \\ \tilde{d}_q \end{bmatrix} \tag{21}$$

Based on differential equations, the small signal circuit model of the 3-1MC with feed-forward decoupling control is built in Fig.10, where:

$$\begin{cases} \tilde{i}_{cc} = \frac{3}{2}f_c(D_d\tilde{i}_d + I_d\tilde{d}_d + D_q\tilde{i}_q + I_q\tilde{d}_q) = \sum_n^4 \tilde{i}_{cn} \\ \tilde{i}_o = \frac{3}{2}f_l(D_d\tilde{i}_d + I_d\tilde{d}_d + D_q\tilde{i}_q + I_q\tilde{d}_q) = \sum_n^4 \tilde{i}_{on} \end{cases} \tag{22}$$

The small signal circuit model is very simple and clear. The input sides of the model are two independent Boost type switch networks in parallel. This greatly simplifies the time-varying, complex mathematical model of the 3-1MC. In addition, regulation without steady-state errors can be achieved. This contributes to the research and design of the closed-loop system.

V. Closed-Loop Control and Controller Design

A. Dual-Loop Control System

In the dq coordinate system, the d axis current and q axis current control the active component and reactive component of the input current independently. However, the reference of the d axis current is a dc signal, so the control variable for the voltage loop should also be a dc signal.

The weighted composite voltage can be expressed as:

$$u_{comp} = f_l u_o + f_c u_c = \frac{h_l^* U_o}{\sqrt{2}}\cos\varphi_o$$

This is proportional to the load voltage RMS value, and the ratio is kept constant. Thus, it can be taken as the control variable for the voltage loop.

According to the small signal circuit model and (16)-(19), the small signal component of the weighted composite voltage $\tilde{u}_{comp}$ is composited by the small signal components of the load voltage and decoupling capacitor voltage. It also has a linear relationship with the small signal of the dc link current. As for the current source inverter, the dc link current determines the load voltage and decoupling capacitor voltage.

In addition, the weighted composite voltage can be calculated by sampling the instantaneous values of the load voltage and decoupling unit voltage. The integral computation for calculating the voltage RMS value is no longer necessary.

Therefore, taking the weighted composite voltage as the feedback quantity can indirectly control the load voltage and

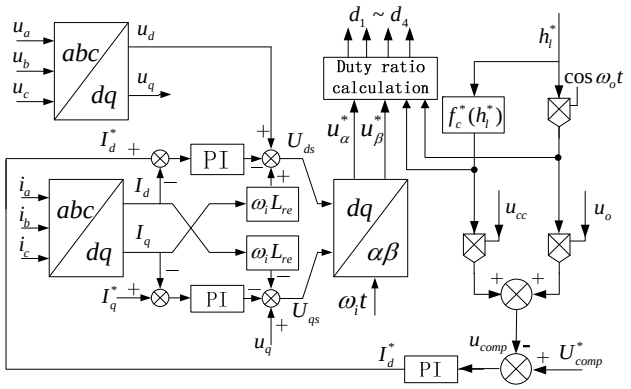

Fig. 11. Control system of 3-1MC based on the weighted composite voltage feedback.

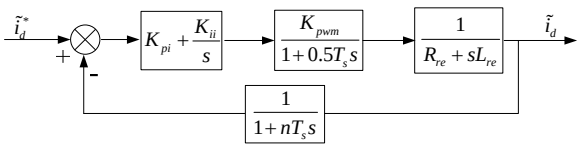

Fig. 12. D axis current loop control.

decoupling capacitor voltage. In addition, its characteristic of rapid calculation will improve the dynamic response speed of the control system.

According to (21), the input current feed-forward decoupling control is employed. Then, the d axis current and q axis current are used to adjust the three-phase active and reactive power. Through the feedback of the weighted composite voltage, the voltage-loop control quantities are dc variables. Therefore, the pi regulation has no steady-state error and the control system design is simplified. Finally, a novel dual-loop control strategy with the weighted composite voltage feedback is proposed. The complete closed-loop control system of the 3-1 MC power decoupling topology is illustrated in Fig. 11.

B. Controller Design

In the dual-loop control, the outer voltage loop varies much slower than the inner current loop. As a result, it is assumed that $\tilde{u}_{comp}^{*}=0$ to design the current loop controller.

To keep the system symmetric, the d and q axis current control should be the same. Taking the d axis control block diagram as an example (shown in Fig. 12), the following presents the analysis and design of the current-loop control parameters.

Where $\frac{K_{pwm}}{1+0.5T_s s}$ is the inertia link of the virtual rectifier, $\frac{1}{R_{re}+sL_{re}}$ is the inertia link of the control-to-current transfer function, $\frac{1}{1+nT_s s}$ is the delay of the current sampling feedback channel, and $k_{ip}+k_{ii}/s$ is the PI controller of the current loop.

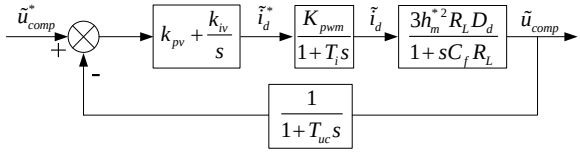

Fig. 13. Outer voltage loop control.

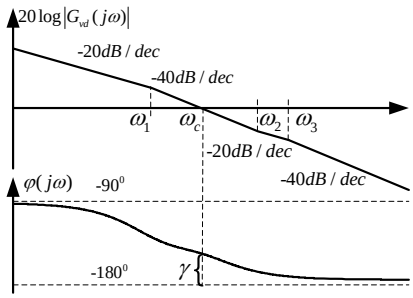

Fig. 14. Bode diagram of voltage open loop transfer function of 3-1MC.

Two little-time inertial links are equivalent to one inertial link. The zero and pole of the large time constant offset each other to improve the regulation speed. Then, its closed-loop transfer function is derived as:

$$\Phi_{id}(s)=\frac{K_{pwm}k_{pi}/T_{is}}{s^2+L_{re}s/T_{is}+K_{pwm}k_{pi}/T_{is}}=\frac{\omega_n^2}{s^2+2\xi\omega_n s+\omega_n^2} \quad (23)$$

Where $T_{is}=0.5T_s+nT_s$ .Then, the scale parameter and the integral parameter are obtained:

$$k_{ip}=\frac{L_{re}}{4\xi^2 K_{pwm}T_{is}} \quad , \quad k_{ii}=\frac{R_{re}}{L_{re}}k_{ip} \quad (24)$$

In this paper, the inductance and parasitic resistance of the ac inductors are $L_{re}=2mH, R_{re}=0.1\Omega$, the PWM frequency is $f_s=10kHz$, and the damping ratio ξ is usually 0.707. Then, the scale parameter and the integral parameter are calculated: $k_{ip}=0.47, k_{ii}=23.5$

The further design for the voltage loop control block diagram is shown in Fig. 13. $1/(1+T_{uc}s)$ is the delay of the voltage sampling feedback channel, $3h_l^{*2}R_L D_d/\left(1+sC_f R_L\right)$ is the $\tilde{i}_d$ -to- $\tilde{u}_{comp}^{*}$ transfer function, $K_{pwm}/\left(1+T_i s\right)$ is the simplified closed-loop transfer function of the current loop, $T_i=L_{re}/k_{ip}$,and $k_{pv}+k_{iv}/s$ is the outer loop PI controller.

The order is reduced by merging little-time inertial links in the same way, and the open-loop transfer function is obtained as follow:

$$G_{vd}(s)=\frac{3D_d h_l^{*2}R_L K_{pwm}k_{iv}(1+k_{pv}s/k_{iv})}{s(1+T_{vs}s)(1+sC_f R_L)} \quad (25)$$

Where $T_{vs}=T_i+T_{uc}$. According to (25), the amplitude frequency characteristics and phase frequency characteristic curves of the outer voltage loop transfer function are given in

Fig. 14. The transfer function is specially designed so that the zero is between two poles, i.e. the outer loop PI parameters satisfy the formula:

$$1/T_{vs} < k_{iv}/k_{pv} < 1/(sC_f R_L) \quad (26)$$

The filter capacitor $C_f = 4.4\mu F$, and the load resistance $R_L = 50\Omega$-150Ω. By combining (26) with Fig. 14, the outer voltage loop PI parameters are designed as $k_{vp} = 0.1, k_{vi} = 60$. Then, the phase angle margin $\gamma = 45^0$-70^0. As a result, the overshoot and adjusting time of the control system can be well balanced.

VI. Simulation of the Closed Loop System

To verify the effectiveness of the presented dual-loop control scheme, simulations of the dynamic process are performed for a 3-1MC with the decoupling unit in Matlab Simulink. The major parameters of the numerical simulation are given as:

$U_{lin} = 45V$, $f_{in} = 40Hz$, $U_o = 150V$, $f_o = 40Hz$,
$C_C = 28\mu F$, $L_{re} = 2mH$, $R_{re} = 0.1\Omega$, $f_s = 10kHz$,
$C_f = 4.4\mu F$, $k_{ip} = 0.47, k_{ii} = 23.5$, and
$k_{vp} = 0.1, k_{vi} = 60$.

Where U_{lin} is the effective value of the line voltage in the three-phase side, and f_{in} is the input frequency.

Consider that disturbances are mainly from the source and load in actual operation. The following part analyzes the dynamic regulation features of the 3-1MC in both disturbance cases.

Load disturbances include sudden load increases and decreases. Simulation waveforms of the input current and voltage, the output load voltage and the decoupling voltage are illustrated in Fig. 15(a) when the load suddenly increases. Since the load resistance decreases from $R_L = 100\Omega$ to $R_L = 50\Omega$, the input current increases twice to maintain the power balance. The load current jumps one time, and consequently the power pulsation absorbed by the decoupling capacitor jumps one time. Then, the maximum voltage of the decoupling capacitor jumps $\sqrt{2}$ times, increasing from 226V to 320V. When the load changes, the output voltage presents a little distortion due to a delay of the closed-loop controllers. As a result, the voltage has a tiny drop. However, it soon settles down to 150V and its THD remains at 4.5%.In the process of adjustment, the input current and decoupling capacitor voltage both transit to the steady state rapidly and smoothly. The input current is still keep in phase with the input voltage and its THD is only 2.7%.

Simulation results when load suddenly decreases are illustrated in Fig. 15(b). When the load resistance increases from $R_L = 50\Omega$ to $R_L = 100\Omega$, the regulating process of the

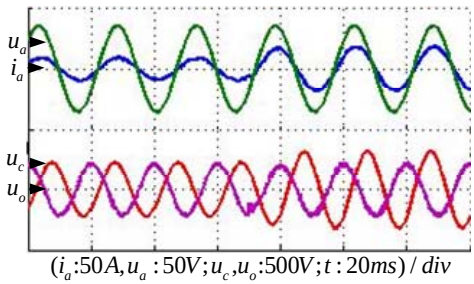

(a) Load sudden increasing.

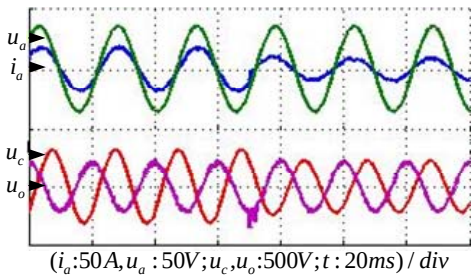

(b) Load sudden decrease.

Fig. 15. Simulation waveforms in load disturbance.

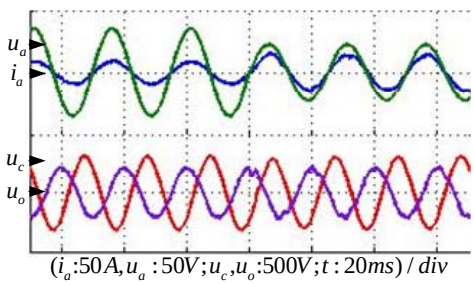

(a) Input voltage sudden decrease.

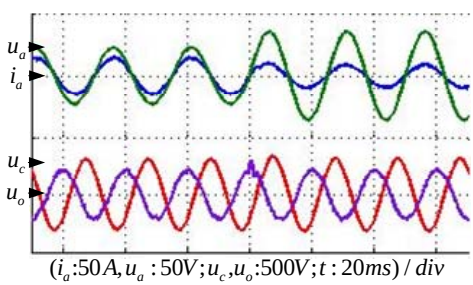

(b) Input voltage sudden increase.

Fig. 16. Simulation waveforms in input voltage disturbance.

input current and decoupling capacitor voltage is exactly opposite to the load increase. Due to the increase of the load resistance and the delay of the closed-loop controllers, the output voltage has an overshoot. However, it soon returns to the 150V steady state. The THD of the output voltage and input current are 3.7% and 3.2%.

The input voltages may sharply increase or decrease. Fig. 16(a) shows the simulation waveforms of the 3-1MC when the input voltage suddenly decreases by 36%. The input current continuously increases to keep the power balance. The output voltage has a little distortion in the changing

Fig. 17. 3-1MC prototype.

moment. However, it returns to the steady state in a cycle. The output impedance remains unchanged. Therefore, the output power and the power pulsation are the same, and the decoupling capacitor voltage basically remains invariant.

Fig. 16(b) shows the simulation waveforms of the 3-1MC when the input voltage suddenly increases by 36%. Regulating the process of the input current is opposite to the input voltage increase. The maximum voltage of the decoupling capacitor voltage remains the same in the changing moment. The output voltage has a slight distortion. However, it quickly regains stability.

It is seen from the above simulation analysis that whether the disturbance is from the load or input source, the closed-loop control system can effectively control the 3-1MC and adjust the input current and output voltage to the steady state in a cycle. In addition, the steady-state output voltage is not affected by disturbances. These results demonstrate that the proposed control scheme performs well at regulating properties. In addition, the changed power pulsation is absorbed completely by the decoupling capacitor throughout the experiment. This proves that the 3-1MC system can implement power decoupling in the closed-loop regulating process.

VII. EXPERIMENT VERIFICATION

The proposed control strategy and the design of the controllers are verified on a 500W prototype of a 3-1 MC with a power decoupling unit, as shown in Fig. 17. The prototype takes a TMS320F28335+CPLD as the core controller. Four-step communication is employed for safe communication.

The hardware circuit is developed with the same parameters as those in the simulations.

A dynamic experimental study is carried out in four aspects: sudden load increase, sudden load decrease, sudden input voltage increase, sudden input voltage decrease. This is done to analyze the regulating capacity and response speed of the 3-1 MC with a power decoupling unit.

In Fig. 18(a), since the load resistance suddenly drops from $R_L = 100\Omega$ to $R_L = 50\Omega$, it takes 2 cycles for the input

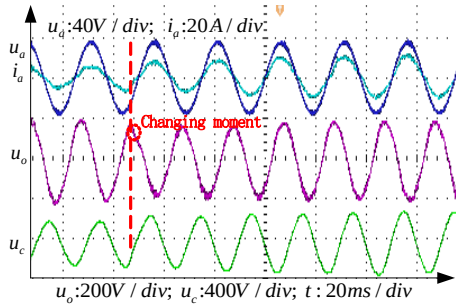

(a) Load sudden increase.

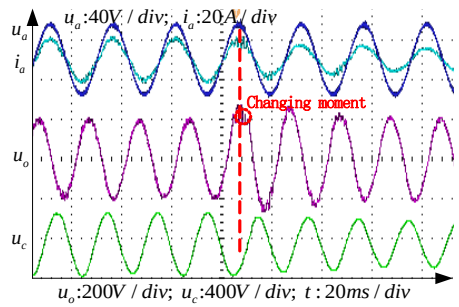

(b) Load sudden decrease.

Fig. 18. Experiment waveforms of load disturbance.

current i_a to reach the steady state. The current RMS value increases from 3.89 A to 7.5 A, the input current and voltage are still in phase, and the PF value is between 0.996 ~ 0.998. Due to the sudden load increase, the output voltage u_o has a slight drop in the changing moment. However, it also returns to 150V in 2 cycles. The input current THD is 3.3% and the output voltage THD is 4.7%. The larger load current leads to a larger power pulsation. Thus, the energy stored in decoupling capacitor is greater and the maximum voltage of the capacitor is increased from 225V to 319V.

Fig. 18(b) shows the experimental waveforms of i_a, u_o, and u_{cc} when the load resistance suddenly increases from $R_L = 50\Omega$ to $R_L = 100\Omega$. i_a, u_o, and u_c return to the steady state in one cycle after the changing moment. At the beginning of the load decreasing, u_o has an overshoot of $\sigma\% = 12\% \sim 15\%$, while the steady output voltage is still 150V. i_a and u_c both transit to the steady state smoothly. The adjusting process is exactly the opposite case of the load current sudden increase. After the dynamic process, the THDs of the output voltage and input current remain at 4.0% and 4.1%, respectively.

The experimental waveforms when the input voltage suddenly increases by 33% and decreases by 33% are shown in Fig. 19(a)-(b).When keeping $R_L = 100\Omega$ and $u_o = 150V$, the input current decreases to 75% and increases to 150% compared with the original value. After the input voltage suddenly changes, i_a is slightly distorted. However, it restores stability in a half cycle.

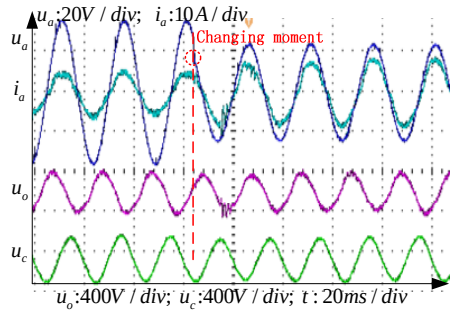

(a) Input voltage sudden decrease.

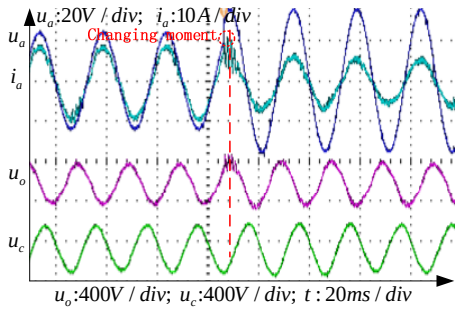

(b) Input voltage sudden increase.

Fig. 19. Experiment waves of input voltage disturbance.

Load voltage u_o has a little distortion due to the effect of the i_a distortion. However, it reaches the steady state quickly. In addition, the THD of u_o is below 5% in the re-steady state. As the power pulsation stays unchanged, u_c is almost not affected by input voltage disturbances, which is consistent with the simulation results.

The experiment indicates that when a load disturbance or input voltage disturbance occurs, the closed-loop control system has a good dynamic regulating capability and a high response speed. Control objects such as the input current, output voltage, and decoupling capacitor voltage are adjusted to the steady state in one half to two cycles after the disturbance occurs. In addition, the PF value of the input current is close to 1 and the output voltage THD<5% in the re-steady state. These results confirm that the proposed control strategy is feasible for the 3-1MC with a power decoupling capacitor.

VIII. Conclusion

Based on an analysis of the relationship between the 3-1MC output load voltage and the decoupling capacitor voltage, this article proposes a novel control strategy that takes the output weighted composite voltage as the outer loop control variable, and realizes the output weighted control of the 3-1MC. Then, using the d and q axis current with feed-forward decoupling control as the current loop control variable, it obtains a unity power factor and a sinusoidal input current. The effectiveness of this strategy has been verified through experiment.

The transfer function expressions and controller design method are deduced through developing and studying the small signal model of a 3-1MC. By using this method to design a 3-1MC closed-loop control system, the control objects such as the input current and output voltage can be adjusted to the steady state in one half to two cycles after disturbances occur. This demonstrates the rapid dynamic response and the strong stability of the system.

Simulation and experimental results confirm that the closed-loop design method based on the proposed strategy is feasible. The system effectively accomplishes power decoupling with a high quality input current and a sinusoidal output voltage. It also demonstrates a fast dynamic adjustment ability.

Acknowledgment

This paper is supported by foundation of Graduate Innovation Center in NUAA, No. kjff 201470, Fundamental Research Funds for the central Universities, and the Joint Funds of the National Natural Science Foundation of China (Grant No. U1233127)

References

[1] N. Nguyen-Quang, D. A. Stone, C. M. Bingham, and M. P. Foster, "A three-phase to single-phase matrix converter for high-frequency induction heating," *Power Electronics and Applications, 13th European Conference on*, pp. 1-10, 2009.

[2] M. Yang, S. Kai, and H. Lipei, "Three-phase to single-phase matrix converter using RB-IGBT," *Transactions of China Electro technical Society*, Vol. 22, No. 3, pp. 91-95, Mar. 2007.

[3] W. B. Zhang and H. J. Ge, "A novel control strategy based on virtual dc voltage feedback for an improved three-phase to single-phase matrix converter," *Applied Mechanics and Materials*, Vol. 294, No. 15, pp. 2452-2458, Feb. 2013.

[4] Y. Miura, S. Kokubo, and D. Maekawa, "Power modulation control of a three-phase to single-phase matrix converter for a gas engine cogeneration system," in *Power Electronic Specialists Conference (IEEE)*, pp. 2704-2710, 2008.

[5] E. Karaman, M. Farasat, F. Niu, and A. M. Trzynadlowski, "Three-phase to single-phase super-sparse matrix converters," in *Applied Power Electronics Conference and Exposition (APEC)*, pp. 1061-1066, 2012.

[6] M. Saito, T. Takeshita, and N. Matsui, "A single to three phase matrix converter with a power decoupling capability," in *Power Electronics Specialists Conference*, pp. 2400-2405, 2004.

[7] T. Yamashita and T. Takeshita, "PWM strategy of single-phase to three-phase matrix converters for reducing a number of commutations," in *The 2010 International Power Electronics Conference*, pp. 3057-3064, 2010.

[8] Y. Furuhashi and T. Takeshita, "Single-phase to three-phase matrix converter with compensation for instantaneous-power fluctuation," in *37th Annual*

Conference on IEEE Industrial Electronics Society, pp. 1572-1577, 2011.
[9] Y. Miura, T. Amano, and T. Ise, "Hybrid control scheme of power compensation and modulation for a three-phase to single-phase matrix converter with a small capacitor," in *International Power Electronics Conference*, pp. 1780-1787, 2010.
[10] Y. Miura, T. Amano, and T. Ise, "Operating characteristics of a three-phase to single-phase matrix converter with hybrid control scheme of power compensation and modulation applied to gas engine cogeneration system," in *Power Electronics and Applications (EPE 2011), Proceedings of the 2011-14th European Conference on*, pp. 1-10, 2011.
[11] Q. Bo and L. Zhengyu, "Small-signal modeling and controller design of three-phase voltage source PWM rectifier," *Transactions of China Electro- technical Society*, Vol. 25 No. 5, pp. 103-108, May 2010.
[12] T. L. Van, D.-C. Lee, "Developing function models of back-to-back PWM converters for simplified simulation," *Journal of Power Electronics*, Vol. 11, No. 1, pp. 51-58, Sep. 2011.
[13] X. Zhang, "Study on the PWM Rectifier and its Control Strategies," Ph.D. Dissertation, Hefei University of Technology, China, 2003.
[14] Z. Wenbin, "The research on power decoupling and control strategy of three-phase to single-phase matrix converter," Nanjing University of Aeronautics and Astronautics, China, 2013.
[15] F. Gao and M. R. Iravani, "Dynamic model of a space vector modulated matrix converter," *IEEE Trans. Power Del*., Vol. 22, No. 3, pp. 1696-1705, Jul. 2007.
[16] X. Liu, Q. Zhang, D. Hou, and S. Wang, "Improved space vector modulation strategy for AC-DC matrix converters," *Journal of Power Electronics*, Vol. 13, No. 4, pp. 647-655, Jul. 2013.
[17] J. Rodriguez, M. Rivera, J. W. Kolar, P. W. Wheeler, "A review of control and modulation methods for matrix converter," *IEEE Trans. Ind. Electron*., Vol. 59, No. 1, pp. 58-70, Jan. 2012.
[18] D. N. Zmood and D. G. Holmes, "Stationary frame current regulation of PWM inverters with zero steady-state error," IEEE Trans. Power Electron., Vol. 18, No. 3, pp. 814-822, May 2003.

Si Chen was born in Yiyang, China, in 1991. He received his B.S. degree in Electrical Engineering and Automation from the Nanjing University of Aeronautics and Astronautics (NUAA), Nanjing, China, in 2013. Since 2013, he has been working toward his M.S. in Civil Aviation Electrical Engineering at NUAA. His current research interests include matrix converter control, and multi pulse rectification technology.

Hongjuan Ge was born in Jiangsu, China, in 1966. She received her B.S. and M.S. degrees in Electrical Engineering from Southeast University, Nanjing, China, in 1985 and 1988, respectively; and her Ph.D. degree in Electric Machines and Electric Apparatus from the Nanjing University of Aeronautics and Astronautics, Nanjing, China, in 2006. Her current research interests include space-vector control of PMMs, AC-AC converters, and airworthiness technology.

Wenbin Zhang was born in Suzhou, China, in 1988. He received his B.S. and M.S. degrees in Electrical Engineering and Automation from the Nanjing University of Aeronautics and Astronautics, Nanjing, China, in 2011 and 2014, respectively. His current research interests include AC-AC power converters, and renewable energy.

Song Lu was born in Nantong, China, in 1990. He received his B.S. degree in Electrical Engineering from Jiangnan University, Wuxi, China, in 2012; and his M.S. degree in Electric Machines and Electric Apparatus from the Nanjing University of Aeronautics and Astronautics, Nanjing, China, in 2015. His current research interests include power electronics and control, and grid-connected matrix converters.